

Section 4: Use Cases

Below are four use cases, which use

- the (regional frequency analysis) RFA-based extreme water levels (EWLs) to map (at city scales) the annual probabilities/frequencies for the NOAA minor (disruptive), moderate (typically damaging), and major (often destructive) high tide flooding (HTF) layer classifications that are nationally calibrated to those used in weather-warning forecasting by NOAA;
- the relative sea level (RSL) projections and the RFA-based EWLs to incorporate trends (e.g., sea level rise projections) into design engineering criteria for risk management and adaptive planning;
- the RSL projections and RFA-based EWL probabilities with maps of NOAA minor, moderate, and major HTF layers to assess current and future vulnerabilities to combined storm and wastewater systems; and
- vertical land motion (VLM) rates inherent to the RSL projections are compared to rates from new satellite technologies at very high spatial resolution to showcase possibilities to monitor current rates from space and further localize the RSL projections.

The goal is to contextualize how the emerging science and this report's datasets can assist in developing products suitable for approaching (mapping, designing, or bounding) important problems in coastal risk assessment and management.

4.1. Mapping of NOAA High Tide Flood Thresholds and Flood Frequencies

High tide flooding²⁹ is increasingly common due to years of RSL rise. NOAA has been 1) documenting changes in minor HTF patterns since 2015, with about 100 NOAA tide gauges along the U.S. coastlines, and 2) providing a yearly coastal HTF outlook for these locations for the coming year,³⁰ as well as projections for the next several decades based on RSL projections from NCA4/Sweet et al., 2017. NOAA has also mapped the three HTF depth-severity (minor, moderate, and major) categories based on the relationship with tide range (Sweet et al., 2018) to show the spatial extent of associated impacts (see Figure 3.7). The minor HTF maps are provided in the NOAA SLR Viewer,³¹ and all three map layers are accessible through NOAA map services.³²

In an effort to provide better flood exposure information, NOAA is developing a product with input from partners (e.g., the Federal Emergency Management Agency [FEMA]) to assign exceedance probabilities using the RFA-based EWLs to the minor, moderate, and major HTF categories as shown for Charleston, South Carolina, and West Palm Beach, Florida (Figure 4.1). The annual event frequency shown for each NOAA HTF “zone” is assigned to the particular flood height. For example, the moderate HTF zone in Charleston is shown as the orange-brown layer in Figure 4.1a, which includes all land elevations between the minor HTF height threshold (0.570 m above mean higher high water [MHHW]; see Table A1.2) and the moderate HTF threshold (0.853 m above MHHW). This moderate HTF zone is expected to be completely (up to 0.853 m above MHHW) at risk of flooding, with an average event frequency between about 1 event/year and 0.2 events/year. A frequency range is provided to partially address the 95% confidence intervals in both the EWL statistics and the mapping data. In the case of local maps, like Charleston and West Palm Beach, the average event frequency for each NOAA HTF layer is a constant across the area shown.

These types of products can help inform the probability of higher-frequency, lower-impact events. As agencies (e.g., FEMA) start to develop products that provide more comprehensive hazard and risk information

²⁹ <https://oceanservice.noaa.gov/facts/high-tide-flooding.html>

³⁰ https://tidesandcurrents.noaa.gov/HighTideFlooding_AnnualOutlook.html

³¹ <https://coast.noaa.gov/slr/>

³² https://coast.noaa.gov/arcgis/rest/services/dc_slr/Flood_Frequency/MapServer

(e.g., graduated flood risk; see The Future of Flood Risk Data³³), there is a need to better define and resolve the probabilities of these more frequent flood conditions. In addition, considering today's height-severity flood thresholds in the face of sea level rise (see Figure 1.3), understanding the event probabilities in this more frequent space is critical. Such information would help graduate the flood probabilities more comprehensively than FEMA's binary 1% annual chance floodplain definition and allow for a more comprehensive picture of structure-level risk.

How Can This Be Done?

The process to spatially assign probabilities again relies on a relationship to tide range (see Figure A2.5), with tide range values obtained by subtracting VDatum's MHHW and mean lower low water [MLLW] modeled tidal surfaces.³⁴ Using VDatum's tide range and the regional regression equations (Figure A2.5) to obtain a local index (u), the EWL return level (or rather, average event frequency) curves for the associated grid are downscaled to individual VDatum grid cells (~100 m) using Equation 1 in Section 3.2. With these downscaled curves, the HTF levels at each VDatum cell—also based on VDatum's tide range (i.e., great diurnal tide range [GT] tide datum) relationships (Sweet et al., 2018)—are intersected with the localized frequency curve (expected values) for the cell in order to determine event frequencies on a cell-by-cell basis. The average event frequencies are then associated with their respective mapped inundation footprints (3–5 m horizontal resolution). To refine the data, they were clipped to the coastal HUC (hydrologic unit code) 12 watersheds³⁵ that overlapped VDatum model data. This was done in order to provide a probability in watersheds that contained source VDatum data only.

The value of these data is that we can now provide not only the mapped inundation extent of each of the three HTF levels (see Figure 3.7) but also the probability, or event frequencies, for each level on high-resolution inundation data (Figure 4.1). By leveraging the relationship between the local indices (u) to GT on a regional basis, the EWL statistics can provide event frequencies for 1) most water levels or flood heights of interest and 2) most locations, even if there is not a local tide gauge nearby to assist coastal managers when planning for potential impacts to their communities. In terms of the mapped product and inherent uncertainties, it should be recognized that the VDatum model's standard error is on the order of 15 cm,³⁶ which is similar to that of the LIDAR elevation data.³⁷ The associated 95% confidence intervals from both VDatum and the LIDAR used in the mapping is then (standard error x 1.96) about 30 cm and similar to that of the EWL at the 1 event/year frequency (0.3 m median) using tide range to spatially derive EWL_{local} (Figure A2.5), although it increases to about 0.9 m at the 0.01 events/year frequency. Thus, it is recommended that these maps be used cautiously in any type of application.

Both NOAA and FEMA are currently exploring methods to further localize the $EWL_{gridded}$ probabilities, such as using NOAA short-term gauges (e.g., Section 3.4) and multidecadal hindcast modeling to develop a higher resolution set of local indices (u). FEMA is working to merge the higher-frequency portion of the EWL distributions (e.g., > 0.05 events/year) with the FEMA EWL stillwater datasets (some of which are shown in Figure 3.5). These efforts will serve, in general, to refine coastal exposure by today's standards and, specifically, minor to major HTF probabilities to better understand and communicate the Nation's coastal flood risk through products such as FEMA's National Risk Index.³⁸

³³ <https://www.fema.gov/fact-sheet/future-flood-risk-data-ffrd>

³⁴ <https://vdatum.noaa.gov/>

³⁵ https://www.usgs.gov/core-science-systems/ngp/national-hydrography/watershed-boundary-dataset?qt-science_support_page_related_con=4 - qt-science_support_page_related_con

³⁶ https://vdatum.noaa.gov/docs/est_uncertainties.html

³⁷ <https://www.usgs.gov/ngp-standards-and-specifications/lidar-base-specification-online>

³⁸ <https://hazards.fema.gov/nri/>

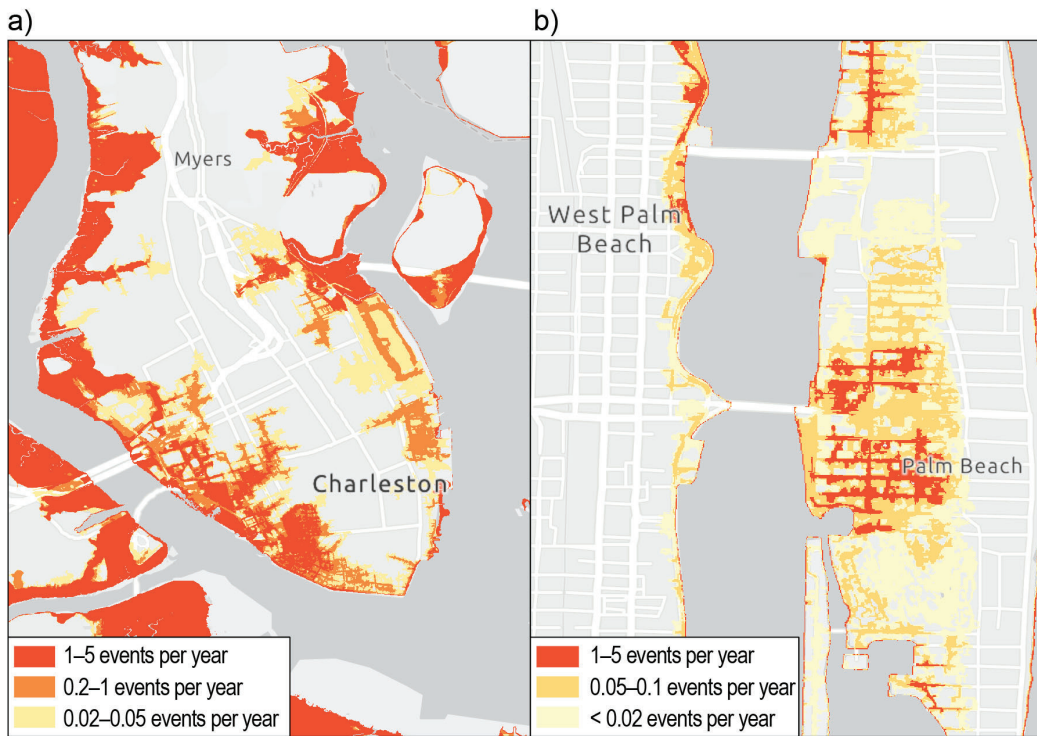


Figure 4.1: Maps of the NOAA minor, moderate, and major high tide flooding layers for a) Charleston, South Carolina, and b) West Palm Beach, Florida (as in Figure 3.7 but providing average event frequencies for each layer). Note: the shoreline on these maps is mean higher high water, but to be useful for decision-making, a conversion to land-based heights (e.g., NAVD88) should be made.

4.2. Application of Scenarios, Observation-Based Extrapolations, and Extreme Water Levels

Because future sea level rise amounts are inherently uncertain, planners and engineers who engage in addressing adaptation to future sea level rise in coastal communities often adopt a scenario approach. Based on several national and regional sea level projections (Hall, Weaver et al., 2019; Parris et al., 2012; USACE, 2014; Hall et al., 2016; Sweet et al., 2017), many communities have developed their own specific scenario sets and guidelines for how to use them. In this section, the application of the regional sea level scenarios (see Section 2) that leverage the newly developed observation-based extrapolations (see Section 2.3) and the EWL probabilities produced using the RFA (see Section 3) are illustrated for representative locations around the United States.

This use case is not meant to provide standardized planning guidance for using information on sea level rise projections; rather, it is provided as an example of applying concepts of time-varying extreme value probabilities due to sea level rise, risk reduction, and adaptive planning that may be used in practice (Salas and Obeysekera, 2014; Salas et al., 2018). One of the primary tasks in coastal infrastructure projects is to determine the design elevation (also known as the return level) of a particular structure (e.g., seawall or building) for a desired level of risk or probability. Such design problems typically require the knowledge of advanced statistical methods associated with extreme values such as those illustrated in the commonly referenced textbook by Coles (2001).

The use case is illustrated for 10 tide gauges around the United States (Figure 4.2). For reference, the upper-bounding scenarios of the observation-based extrapolations for 2050 (see Table 2.2) and the RFA-based EWL distribution parameters (Section 3) are provided in Table 4.1. The EWL probability parameters are necessary to replicate this use case, and they are specifically from a Generalized Pareto Distribution (GPD) peaks-

over-threshold approach (Coles 2001): a) the local Index, u ; b) rate of exceedances above the local index, λ ; c) scale, σ_{RFA} ; and d) shape, ξ (see Section A2 for more details). In the examples below, the upper-bounding scenario is used (Figure 4.3a) with the corresponding return level curves for the selected tide-gauge locations (Figure 4.3b).



Figure 4.2: Tide gauges selected for the application of sea level scenarios and extreme water level methods.

Table 4.1: Tide-gauge locations, scenarios bounding the observation-based extrapolations, and the extreme value distribution Generalized Pareto Distribution (GPD) model parameters estimated using the regional frequency analysis (RFA).

Tide-gauge location details			Upper-bounding scenarios circa 2050 of the observation-based extrapolations	RFA-based GPD parameters			
NOAA ID	Location	Region	Upper Bound	Local Index u	λ	σ_{RFA}	ξ
1612340	Honolulu, HI	Haw.	Int	0.248	3.19	0.218	0.066
8518750	The Battery, NY	NE	Int	0.546	2.98	0.261	0.179
8638610	Sewells Point, VA	NE	Int	0.502	2.95	0.332	0.067
8723214	Virginia Key, FL	SE	Int-High	0.284	3.00	0.152	0.251
8726520	St. Petersburg, FL	E. Gulf	High	0.337	2.99	0.266	0.354
8729840	Pensacola, FL	E. Gulf	High	0.345	2.85	0.212	0.456
8771450	Galveston Pier 21, TX	W. Gulf	Int-High	0.366	2.75	0.289	0.340
9410660	Los Angeles, CA	SW	Int-High	0.472	3.21	0.150	-0.063
9414290	San Francisco, CA	SW	Int-High	0.375	3.15	0.211	0.038
9447130	Seattle, WA	NW	Int	0.541	3.07	0.233	-0.110

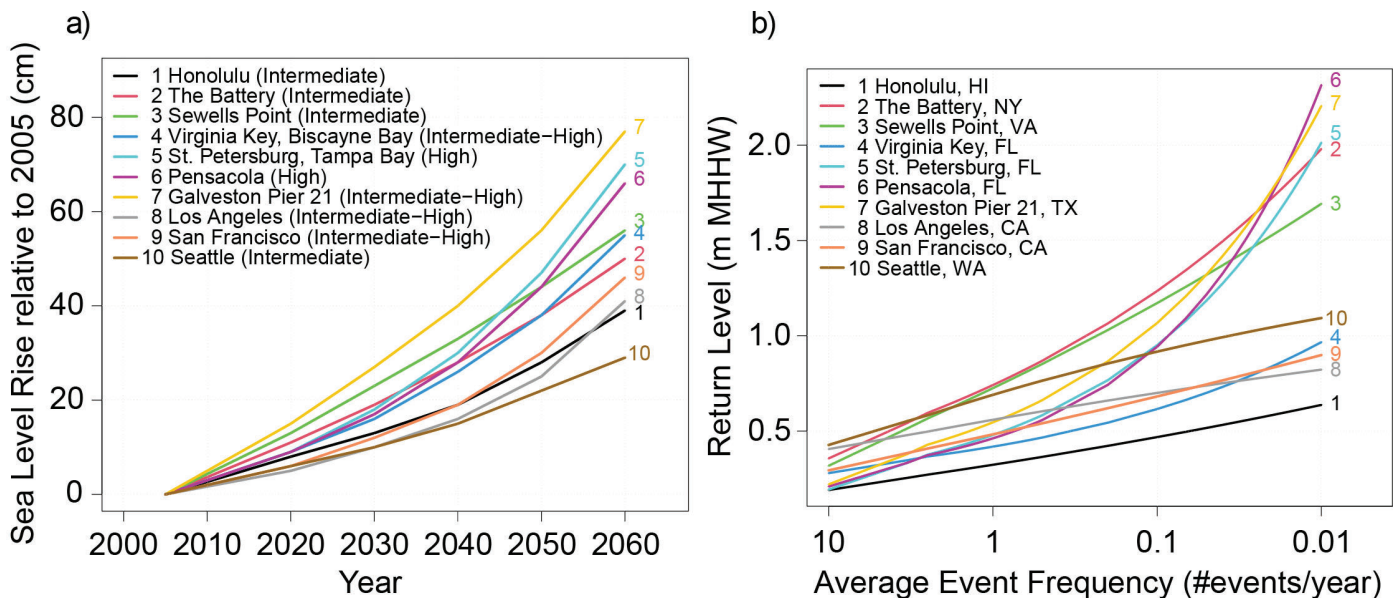


Figure 4.3: a) RSL projections for the scenarios providing the upper bound to observation-based extrapolations to 2060 for the selected tide gauges. The corresponding scenario for each tide gauge is shown in parentheses in the legend. b) RFA-based EWL (see Section 3) return level curves relative to the 1983–2001 MHHW tidal datum. Notes: (1) to be useful for decision-making, a conversion to land-based heights (e.g., geodetic datum such as NAVD88) should be made. (2) Average event frequency (x-axis label) is the reciprocal of average recurrence interval, which is also known as return period.

As shown in Figure 4.3a, 2005 is the reference year for the projection scenarios. However, the return level curves shown in Figure 4.3b are referenced to the year 2000. The return level curves are first adjusted to the year 2005 by raising the curves by an amount equivalent to the local trend in the flood index (u) from 2000 to 2005 (see Table A1.3). Alternatively, the RSL offsets (see Table A1.2) could be applied, with differences between the two insignificant to the results here.

Accounting for Time-Varying Relative Sea Level Rise

A particular scenario depicts the changes in RSL at a selected location. A common assumption is that as RSL rises, the EWLs also increase, and that must be accounted for in the changing behavior of the probability distribution of the EWLs. One approach for developing a time-varying extreme value distribution is to assume that one or more parameters (location, scale, and shape) are functions of time or some other covariate (e.g., El Niño–Southern Oscillation index; Coles, 2001; Menendez and Woodworth, 2010). When two or more parameters evolve with time (i.e., strong nonstationarity), the paradigm shifts from a “stationary” approach, typically used for planning infrastructure until recently, to one reflecting significant temporal change in the probability distribution. A common practice is to remove the trend in the extreme dataset and then to assume the distribution of the detrended extremes to be stationary. This approach is similar to the case when only the location parameter is varying with time and the other parameters are constant.

In the ensuing sections, it is assumed that only the location parameter (i.e., local index, u , in GPD) changes as a function of RSL (i.e., per the specified sea level scenario). This may be expressed as

$$F(z) = GPD(u(RSL), \tilde{\sigma}, \xi)$$

where u is the RFA/GPD local index that is a function of RSL, and $\tilde{\sigma}$ and ξ are scale and shape parameters, respectively, which are assumed to be constant over time. However, this assumption does not preclude the analysis of using a higher degree of temporal variability (e.g., both u and $\tilde{\sigma}$ are functions of RSL or some other covariate). As a consequence of the above assumption, the local index u is adjusted by a magnitude δ (i.e., the regional mean sea level change from the reference year) obtained from a selected scenario.

For planning infrastructure using the scenario’s RSL projections and the EWL probabilities, two approaches are illustrated: 1) recurrent flood frequency and 2) time-varying average recurrence interval (ARI; which is the reciprocal of average event frequency [AEF]) and risk.³⁹ While the infrastructure designs are based on a variety of factors, one or both of these approaches may be used to support that process (e.g., height of a sea-wall or base-flood elevation). In this use case, the term “flood” could pertain to a particular NOAA HTF level or an arbitrary probabilistic EWL level, although not necessarily to imply a meteorological (e.g., storm) event.

Designs Based on Recurrent Flood Frequency

In many U.S. coastal locations, the frequency of flooding is increasing, mostly due to rising sea levels (Sweet et al., 2021). A community may tolerate infrequent flooding initially, but at some point, when the sea level rise is significant, the flooding frequency will increase, which in turn may exceed that community’s risk tolerance for flooding. Using the extreme value distributions and the sea level scenarios, it is possible to predict the time-varying change in frequency (e.g., as in Figure 3.9). In case of the GPD, the recurrent flood frequency (number of exceedances above a return level [z]) may be computed as (Buchanan et al., 2017)

$$N(z, \delta) = \lambda \left(1 + \frac{\xi(z - [u + \delta])}{\bar{\sigma}} \right)^{-\frac{1}{\xi}} \text{ for } \xi \neq 0$$

where δ is the change in RSL (relative to the project construction year) obtained from Figure 4.3a.

In the example used here, the planning problem may be stated as follows: What should the initial return level (used for the design) be to ensure that the recurrent flood frequency is limited to a specified number of events at the end of the design life? It is now possible to lay this out graphically, as shown in Figure 4.4 for two tide gauges (Sewells Points, Virginia, and Galveston Pier 21, Texas).

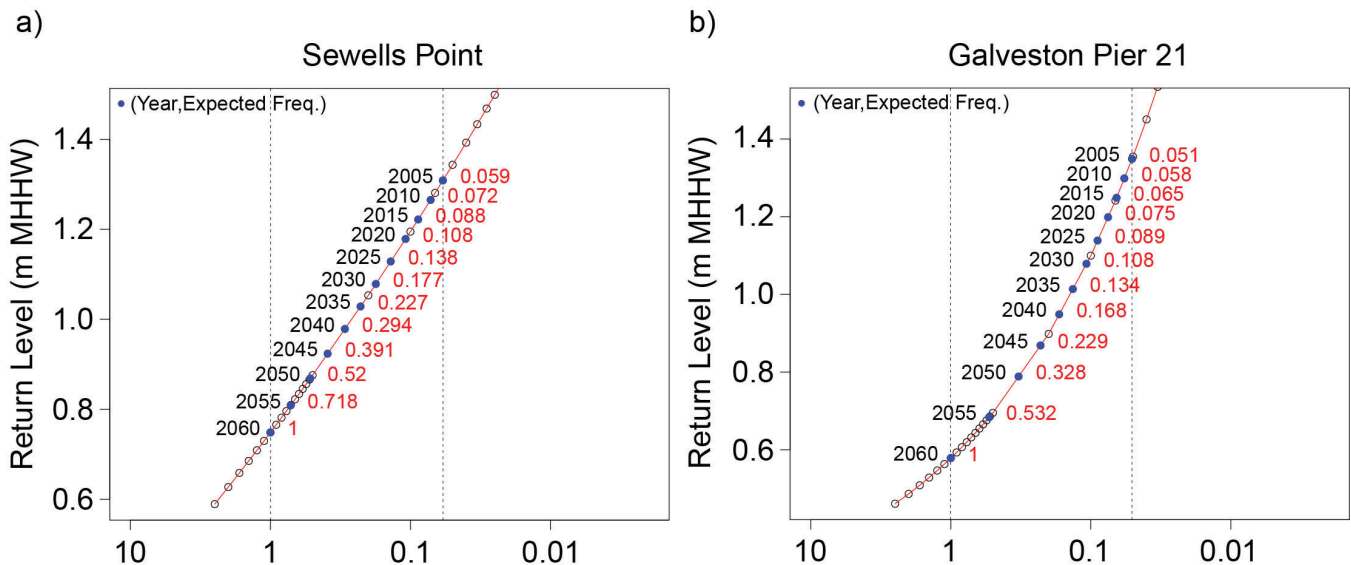


Figure 4.4: Recurrent flood frequency estimates for a) Sewells Point (Norfolk), Virginia, and b) Galveston Pier 21, Texas. For both, the relative sea level projection for the scenarios and the return level are the same as in Table 4.1. Note: to be useful for decision-making, a conversion of the return level to land-based heights (e.g., geodetic datum such as NAVD88) should be made.

In Figure 4.4, the number to the right of each point along the curve shows the recurrent flood frequency, N, corresponding to the year indicated on the left. For this example, it was assumed that by 2060, the desired value of N = 1, and the design AEF necessary for this criterion, is indicated in Figure 4.4 (AEF = 0.06 events/year for Sewells Point and AEF = 0.05 events/year for Galveston Pier 21). The corresponding design return levels are 1.31 m and 1.35 m, respectively, relative to MHHW datum. A summary of results for all 10 tide

³⁹ In the context of Section 4.2, risk is defined as the probability of one or more events exceeding a given height threshold over the life of a project.

gauges is shown in Table 4.2. The design average event frequency required in 2005 to meet the flood frequency criteria shows significant variability across the sites. The design return level depends on two factors: 1) the magnitude of the sea level rise from 2005 to 2060 (end of the design life); and 2) the slope (a function of the scale and shape parameters) of the return level curve (Figure 4.3b).

Table 4.2: Summary of design parameters to constrain the average event frequency, N, to 1 per year by 2060 (end-year of the design life). The 2005–2060 RSL projections are the local values associated with the scenarios providing the upper bound to the regional observation-based extrapolations shown in Table 2.2. Note: to be useful for decision-making, a conversion of the return level to land-based heights (e.g., geodetic datum such as NAVD88) should be made.

NOAA ID	Location	Relative Sea level rise (in meters from 2005 to 2060)	Return level (m above 1983–2001 MHHW) corresponding to AEF = 1 year	Return level (m above 1983–2001 MHHW) required in 2005 to ensure N = 1 by 2060	Design average event frequency (events/year) required in 2005 to achieve N = 1 by 2060
1612340	Honolulu, HI	0.39	0.33	0.72	<0.01
8518750	The Battery, NY	0.50	0.76	1.26	0.10
8638610	Sewells Point, VA	0.56	0.75	1.31	0.06
8723214	Virginia Key, FL	0.55	0.44	0.99	0.01
8726520	St. Petersburg, FL	0.70	0.49	1.19	0.05
8729840	Pensacola, FL	0.66	0.47	1.13	0.06
8771450	Galveston Pier 21, TX	0.77	0.58	1.35	0.05
9410660	Los Angeles, CA	0.41	0.57	0.98	<0.01
9414290	San Francisco, CA	0.46	0.49	0.95	<0.01
9447130	Seattle, WA	0.29	0.70	0.99	0.05

Design Based on Time-Varying Exceedance Probabilities

Average recurrence interval is used to describe EWL probabilities in the following examples to directly relate to and build off of a couple of recent, relevant focused studies on the topic. Interpretation of the results should follow guidelines of the U.S Army Corps of Engineers (USACE, 1994).

In current practice, the projects with a longer design life (> 25 years) typically use a low average event frequency (<0.1 events/year) or, equivalently, a high/long ARI (> 10 years or more). At high recurrence intervals, the peaks-over-threshold and the annual maxima recurrence intervals converge (Langbein, 1949), although not necessarily where tropical storm surges are present (Wahl et al., 2017). Revisiting the concepts of traditional ARI and risk concepts for annual maxima in time-varying frameworks has been addressed recently (e.g., Salas and Obeysekera, 2014). The application of time-varying ARI and risk concepts is illustrated by converting the GPD model to an equivalent annual maxima model, which in this case is the GEV distribution. The equivalent annual-maxima modeling approach, as used here, will also facilitate the direct application of emerging risk and recurrent interval concepts already developed for situations of time-varying extreme probabilities (Salas and Obeysekera, 2014; Salas et al., 2018; Obeysekera and Salas, 2020).

The cumulative distribution function (CDF) of the GEV model of annual maxima is expressed as

$$F(z) = \exp \left\{ - \left[1 + \xi \left(\frac{z - \mu}{\sigma} \right) \right]^{-\frac{1}{\xi}} \right\}$$

where μ , σ , ξ are the location, scale, and shape parameters of the GEV (Coles 2001).

For computing u , the local index is further adjusted to reflect the translation of the return level curve from 2000 to the reference year (i.e., 2005). The GEV scale parameter, $\sigma = \tilde{\sigma}\lambda^\xi$, where the at-site scale parameter $\tilde{\sigma}$, is computed as $\tilde{\sigma} = \sigma_{RFA}^* u$. For this use case, the adjusted local index is computed as $u_{adj} = u * s$ (2005–2000), where s is the trend of the local index u at the site (see Table A1.3). If desirable, other adjustment procedures may be used. Finally, the time-varying GEV model assumes that only the location parameter, μ , changes with sea level change, δ and the time varying annual extreme value distribution is given by

$$F^t(z, \delta) = \exp\left\{-\left[1 + \xi \left(\frac{z - (\mu + \delta)}{\sigma}\right)\right]^{-\frac{1}{\xi}}\right\}$$

The exceedance probability, p_t , which corresponds to an initial return level (z_{q0} , initial design), changes with time because of the rising RSL, δ (Figure 4.5). Consequently, the ARI is not a fixed measure but decreases with increasing sea level.

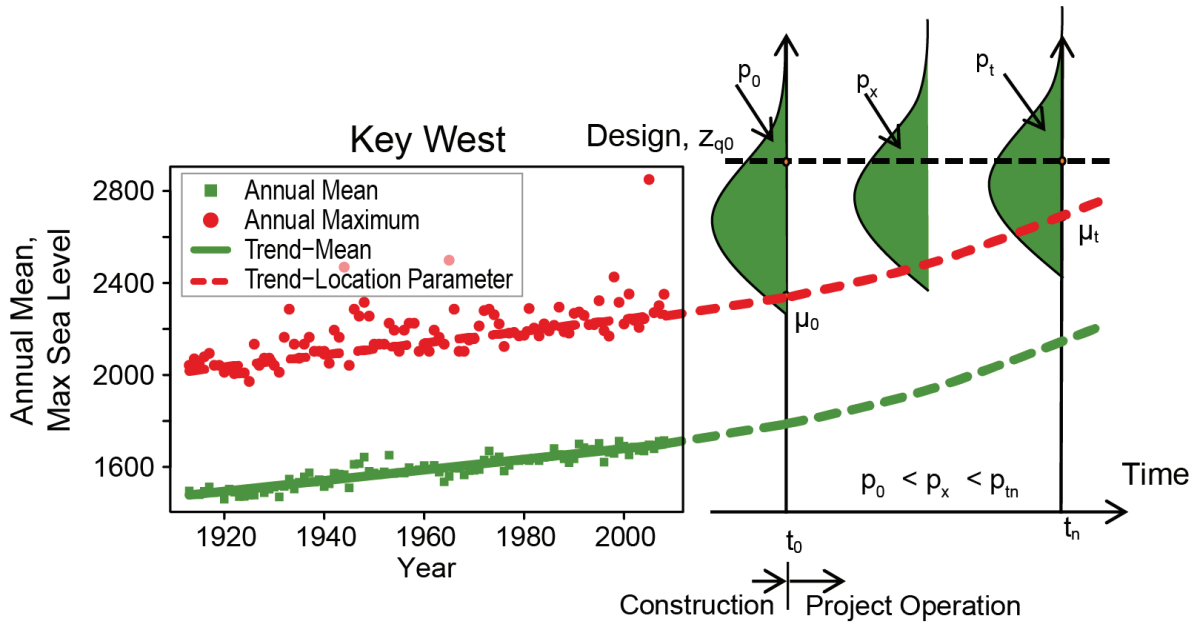


Figure 4.5: Conceptual illustration of increasing exceedance probability (hence decreasing average recurrence interval) that assumes that the location parameter is a function of the magnitude of the relative sea level rise.

The traditional concept of the ARI is the average waiting time for between two successive exceedances of the return level. Using the same definition but in a time-varying exceedance probability framework (Figure 4.5), an equivalent measure of ARI (T) may be derived as (Cooley, 2013; Salas and Obeysekera, 2014)

$$T = 1 + \sum_{x=1}^{\infty} \prod_{t=1}^x (1 - p_t)$$

where $p_t = 1 - F(z, \delta)$ is the time-varying exceedance probability. If a project is designed for a return period, $T_0[t = t_0]$, then $T < T_0$ implies that the actual recurrence interval due to rising RSL will be less.

The methods described in the preceding paragraphs are applied to the 10 tide-gauge locations shown in Figure 4.2. For illustration, it was assumed that the projection scenario for each tide gauge would continue beyond 2060. However, the methodology described above can be used with any other scenario. The derived GEV parameters for each gauge are shown in Table 4.3.

Table 4.3: The parameters of generalized extreme value computed using the peaks-over-threshold Generalized Pareto Distribution model (Coles 2001).

NOAA ID	Location	At-site scale parameter	Local index adjustment from 2000–2005 (m)	GEV location parameter	GEV scale parameter	GEV shape parameter
1612340	Honolulu, HI	0.054	0.007	0.330	0.058	0.066
8518750	The Battery, NY	0.142	0.016	0.757	0.173	0.179
8638610	Sewells Point, VA	0.167	0.023	0.748	0.179	0.067
8723214	Virginia Key, FL	0.048	0.026	0.444	0.063	0.251
8726520	St. Petersburg, FL	0.090	0.014	0.494	0.132	0.354
8729840	Pensacola, FL	0.073	0.012	0.474	0.118	0.456
8771450	Galveston Pier 21, TX	0.106	0.033	0.579	0.149	0.340
9410660	Los Angeles, CA	0.071	0.005	0.565	0.066	-0.063
9414290	San Francisco, CA	0.079	0.010	0.492	0.083	0.038
9447130	Seattle, WA	0.126	0.010	0.701	0.111	-0.110

The ARI curves, T , as a function of T_0 , for all 10 tide gauge locations are shown in Figure 4.6a. This figure demonstrates that, in all cases, the actual ARI is less than the design recurrence interval. For instance, for a location near Pensacola, Florida, if a project is designed for $T_0 = 100$ years, the actual ARI, due to future RSL rise (Table 4.1, “Upper Bound” column), is only about 50 years. As another example, for a location near The Battery, New York City, a project may need to be designed for $T_0 = 90$ years if the desired ARI under its associated (Table 4.1, “Upper Bound” column) RSL rise scenario is 40 years.

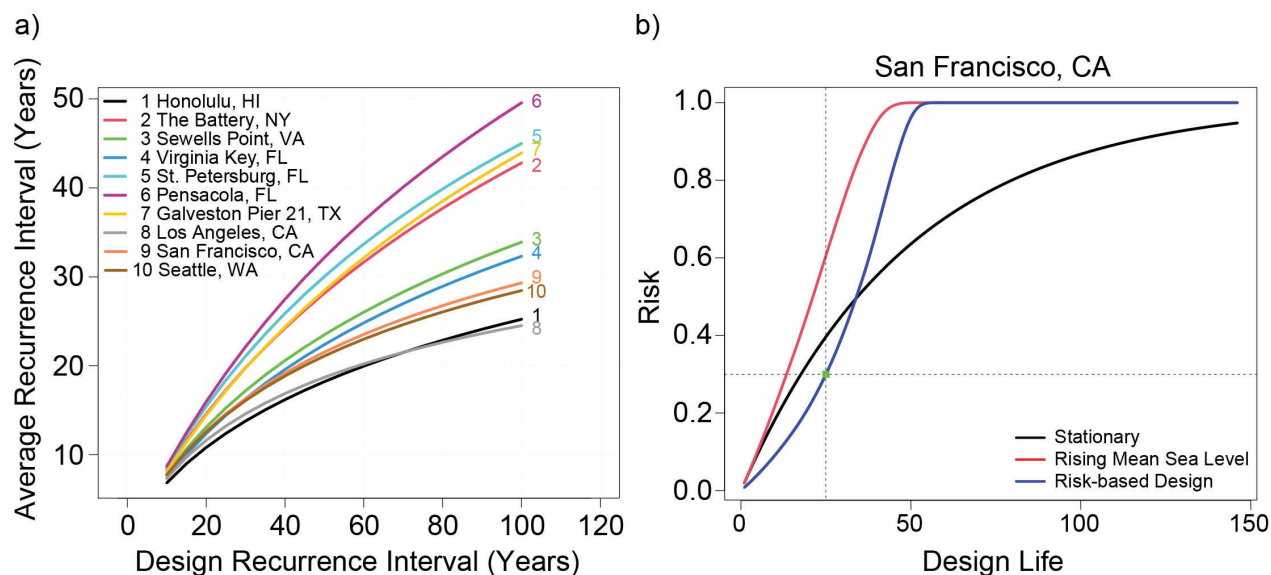


Figure 4.6: a) Average recurrence interval (due to rising RSL) curves (T versus T_0) at each tide gauge using the selected scenario’s RSL projection (see Table 4.1). b) Risk curves as a function of design life: stationary (black curve), actual risk resulting from incorporating the site’s RSL scenario projection (red curve), and risk curve for a specific risk (blue curve).

Risk-Based Design

Under stationary conditions, the risk (defined as the probability of one or more exceedances above the design elevation) is a function of the life of the project, n . The risk formula under stationarity is given by $R = 1 - (1 - 1/T_0)^n$. For example, there is about a ($R = 0.26$) 26% chance of experiencing an event with an ARI of (T_0) 100 years over the course of (n) 30 years under a non-changing (stationary statistical) environment. As the length of the design life increases, risk also increases. Under conditions of time-varying exceedance probability, p_t , the risk (R) formula is (Salas and Obeysekera, 2014)

$$R = 1 - \prod_{t=1}^n (1 - p_t)$$

With rising relative sea levels, p_t increases, and the risk is higher than that under stationarity. This increase in risk is illustrated for the San Francisco, California, tide gauge in Figure 4.6b when the initial design, $T_0 = 50$ years (the event level with a 50-year ARI). The black curve in Figure 4.6b shows the increasing risk as the design life becomes longer even under stationarity. For instance, if the design life, equals 25 years, this risk is about 0.4 (40%). However, when the local sea level rise scenario is incorporated, the risk over a given life of the project increases more rapidly, exceeding the corresponding risk under stationarity (see red curve in Figure 4.6b). In the above example, when $n = 25$ years, the risk will increase to about 60% due to the RSL scenario projection. Moreover, the RSL rise causes the risk to approach 100% ($R = 1$) when the design life is about 50 years or more. In the risk-based design approach, one can specify the tolerable risk and determine the initial design period (or return level).

One option is to design a project in such a way that the resulting increasing risk profile due to application of the scenario's RSL projection is at or below that under stationarity. While the risk-reduction approach described below is illustrated for a selected RSL scenario for the future, it can be implemented for multiple scenarios, leading to a variety of risk-reduction options depending on the future RSL scenarios. In such a broader application, a risk-based framing founded on risk tolerance may be adopted.

Considering uncertainty in the sea level rise projections, one may wish to approach the problem using concepts of dynamically adaptive planning. In the example shown in Figure 4.6b (blue curve), two parameters are specified to illustrate this concept. First, it is assumed that the project will be constructed in, for example, two or more phases. Considering such a planning assumption, phase I is 25 years long (i.e., $n = 25$ years), and the maximum tolerable risk during this phase is 0.3 (30%), as opposed to the 60% risk mentioned above. The blue curve shows the risk profile for such a design. This curve was computed by constraining $R = 0.3$ when $n = 25$, as shown by the green dot in Figure 4.6b. The implication of this adaptive approach is that the initial return level will need to increase from 0.84 m MHHW to 0.93 m MHHW (Table 4.4), and the corresponding initial ARI has to increase from 50 years to 125 years. In this approach, one must also assume that the project will be expanded after that initial period, and measures must be adopted to prevent locking in the design and preempting the planners from expanding it into a bigger project after the initial 25-year period. For example, the foundation design of the project may need to assume the eventual capacity expansion and allow for it in the initial design. This approach of dynamically adaptive planning is becoming increasingly popular as a way to deal with deep uncertainties associated with sea level rise.

Table 4.4 shows that with a relatively small increase in initial design elevation, the risk can be managed to a desirable level. In this example, however, the ultimate design (at the end of the full design life; e.g., 50 or 100 years) needs to be assessed to ensure that resources (e.g., land) that may be needed for the build-out are considered.

Table 4.4: Results of the risk-based design for all tide gauges shown in Figure 4.2. Average recurrence interval (ARI) is listed and is the reciprocal of average event frequency. Values in the last column have been rounded to the closest 5-year interval. Note: to be useful for decision-making, a conversion of the return level to land-based heights (e.g., geodetic datum such as NAVD88) should be made.

NOAA ID	Location	Design return level for $T_0 = 50$ years (m above MHHW)	Design return level to constrain risk to 30% over a 25-year period (m MHHW)	Average recurrence interval (ARI) of the design to constrain probability (risk) to 30% over a 25-year period
1612340	Honolulu, HI	0.59	0.69	>100
8518750	The Battery, NY	1.74	1.95	90
8638610	Sewells Point, VA	1.55	1.75	>100
8723214	Virginia Key, FL	0.78	1.00	>100
8726520	St. Petersburg, FL	1.61	1.88	80
8729840	Pensacola, FL	1.75	2.09	75
8771450	Galveston Pier 21, TX	1.79	2.13	85
9410660	Los Angeles, CA	0.79	0.86	>100
9414290	San Francisco, CA	0.84	0.93	>100
9447130	Seattle, WA	1.05	1.13	>100

4.3. Growing Risk to Combined Storm and Wastewater Systems from Sea Level Rise

Sea level rise is causing HTF to become more severe—more frequent, deeper, and more widespread—in terms of its impacts (Sweet et al., 2021). Coastal areas that are not exposed to HTF now may become so in the coming decades. As the footprint of flooding expands, water from adjacent estuaries and bays will flood into communities and encounter previously unaffected urban infrastructure.

Many places already see backflow from tidal waters through stormwater pipes that spill out of catch basins into neighborhood streets. Cities with combined sewer systems often have backflow preventers on their vulnerable outfall pipes (EPA, 1995a, 1995b). However, combined sewers will be open to inflow from surface flooding. If floodwater in the streets encounters a catch basin that connects to a combined sewer system, then high tide waters will enter the sewer. At best, the tide waters will be on their way to the sewage treatment plant; at worst, a combined sewer outflow would be triggered if the sewer pipes cannot handle the volume of water.

While Camden, New Jersey, has taken action to prevent runoff from entering its system,⁴⁰ tidal inflow is a novel problem. Identification of risks like this can provide lead time to take adaptation actions. Still, in some combined sewer communities, such as Camden, the onset of risk can arrive well before midcentury. Mapping shows that minor HTF at a height of 0.58 m above current MHHW tidal datum (Table A1.3) begins to have a footprint in Camden neighborhoods served by combined sewers (red shade in Figure 4.7, spanning from MHHW to 0.58 m [1.9 feet] above MHHW; locations are provided by the New Jersey Department of Environmental Protection⁴¹). By the time the tide reaches the moderate (0.86 m above MHHW) and major

⁴⁰ <https://www.epa.gov/arc-x/camden-new-jersey-uses-green-infrastructure-manage-stormwater>

⁴¹ <https://njdep.maps.arcgis.com/apps/Viewer/index.html?appid=70dd49de342949ca933e840d0c530fc7>

(1.25 m above MHHW) HTF levels, the extent of flooding increases dramatically, and many intersections will be flooded.

The Camden region currently (circa 2020) experiences

- about 2 events/year (or about 4 days/year per Figure 3.8b) of minor HTF;
- 0.2 events/year of moderate HTF; and
- 0.03 events/year of major HTF,

based on the EWL_{local} directly across the Delaware River at the NOAA tide gauge in Philadelphia. The EWL-based probabilities support actual observations in 2020, when the Camden/Philadelphia region experienced 4 days of minor HTF, with 4–8 days projected to occur in 2021 (Sweet et al., 2021).

Considering the Intermediate scenario, which is the upper-bounding scenario for this region's RSL observation-based extrapolations (see Table 2.2), a rise of 0.19 m by 2030 (measured since 2005) is projected to result in

- 5–10 events/year (on the order of 10–20 days/year) of minor HTF,
- 0.6 events/year of moderate HTF, and
- 0.07 events/year of major HTF.

By 2050, a 0.38 m RSL rise is projected (above 2005 levels) for this area, resulting in

- >10 events/year (perhaps >20 days/year) of minor HTF,
- about 3 events/year (6 days/year) of moderate HTF, and
- 0.3 events/year of major HTF.

So, within about the next 30 years (by 2050), a surface flood regime shift with subsurface impacts is projected to occur in Camden, considering current RSL rise trajectories. By then, moderate and major HTF (flooding upwards of 0.9 m and 1.2 m above MHHW, respectively) is projected to occur with similar frequencies/probabilities as minor (about 0.6 m above MHHW) and moderate HTF occur today. With nearly 4 high tides per event (1 event lasts about 2 days; 2 high tides occur almost every day), this implies that by 2050, upwards of 80 tides per year or more at the minor HTF level are projected, with about 12 of those tides per year exceeding the moderate HTF level and a 0.3 events/year frequency of major HTF flooding. Any time street intersections are underwater, tidal waters could flow down catch basins into the combined system (Figure 4.7). Beyond 2050, HTF frequency, depth, and extent will continue to grow. It is unclear how this increased flood frequency will affect the combined sewer system's functionality and surrounding water quality.

● Combined Sewer Outfall
 ■ Minor
 ■ Moderate
 ■ Major

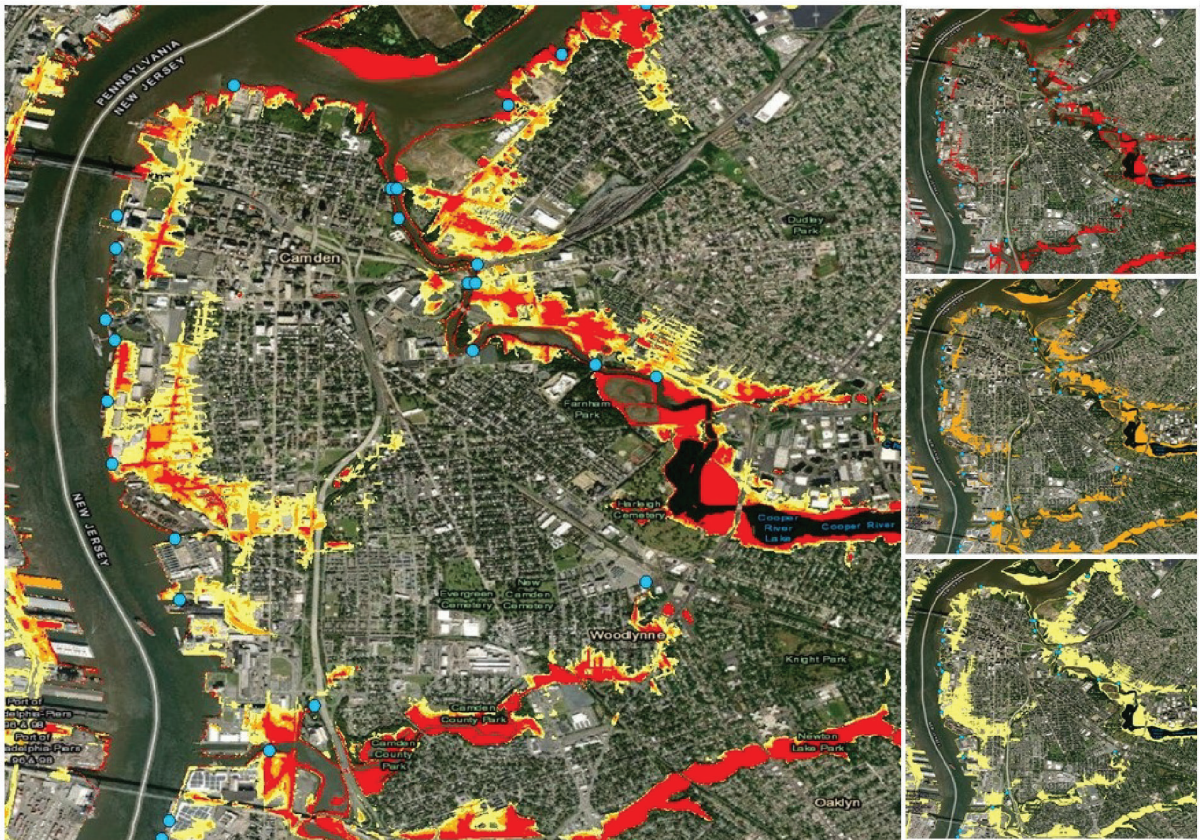


Figure 4.7: Location of combined stormwater and sewer system outfalls that are likely draining regions exposed to HTF within the Camden, New Jersey, region, with the minor (red: MHHW to 0.58 m [1.9 feet] above MHHW), moderate (orange: MHHW to 0.86 m [2.8 feet] above MHHW), and major (yellow: MHHW to 1.25 m [4.1 feet] above MHHW) HTF layers stacked in the enlarged map and individual layers mapped to the right. Note: heights are relative to the 1983–2001 tidal epoch, and to be useful for decision-making, a conversion to land-based heights (e.g., NAVD88) should be made.

4.4: Use of InSAR Technology for Determining Regional Vertical Land Motion and Its Suitability for Computing Long-Term Sea Level Rise Projections

Vertical land motion is an important component of RSL rise, leading to changes in the height of the ocean relative to land. Vertical land motion is not a singular phenomenon but instead results from various processes that display different patterns in space and time. These patterns have different impacts from place to place, especially in coastal settings where many of them operate at the same time and can serve to either increase RSL (subsidence) or decrease RSL (uplift). For much of the coastal United States, subsidence is driven on local scales by both natural processes, such as compaction of river sediments, and unnatural, human-caused reasons, such as groundwater and fossil fuel withdrawal; on larger scales, subsidence is driven by glacial isostatic adjustment (GIA). On the other hand, in some regions, such as southern Alaska, GIA leads to high rates of uplift in coastal regions. For example, Grand Isle, Louisiana, has experienced more than 0.9 m (3 feet) of RSL rise, whereas Juneau, Alaska, has experienced more than 1.2 m (4 feet) of RSL fall based on a 100-year historical linear rate value,⁴² in large part due to VLM. For perspective, the national median RSL rise along U.S. coastlines during this 100-year period was about 0.25–0.30 m (see Figure 1.2b).

⁴² <https://tidesandcurrents.noaa.gov/sltrends/>

Accurate future projections of VLM require an understanding of and accounting for the underlying processes and the time and space scales on which they vary. In this report, VLM projections are based in part on analysis of past observations. Vertical land motion rates are estimated at tide-gauge locations as well as at 1-degree grids using a statistical model of tide-gauge observations (Kopp et al., 2014; Sweet et al., 2017; Fox-Kemper et al., 2021; Garner et al., 2021). The model assesses RSL change across the global tide-gauge network⁴³ with data through about 2019 and separates the tide-gauge observations into 3 modes: 1) a global rise signal (Dangendorf et al., 2019), 2) a long-term linear—but regionally varying—rate, and 3) local effects that vary in time and by region. It is the second mode that defines this report’s linear VLM rates, which have been incorporated into the RSL projections for each GMSL rise scenario. These rates are assumed to be linear over the past record and to persist linearly into the future over the length of the projected record. Assumed persistence may not necessarily be valid over the long term (e.g., if groundwater pumping ceases) but may be necessary due to a lack of data. As shown in Figure 4.8a, high rates of subsidence are estimated along the entire Gulf Coast, and moderate rates of subsidence are assessed along the entire East Coast. On the other hand, high rates of uplift are estimated for the southern coast of Alaska.

Over the past couple of decades, GPS stations have provided estimates of VLM in coastal areas across the United States. These GPS-based VLM estimates provide a comparison to the VLM rates in this report, albeit with a couple of caveats. First, the record lengths over which the GPS-based estimates are computed are significantly shorter than the tide-gauge data records used to infer the VLM rates in this report. Second, many tide-gauge locations do not have a co-located GPS station. While it is not possible to extend the record lengths of the available GPS measurements, the second challenge has been addressed using the GPS-imaging technique discussed in Hammond et al. (2021), which leverages the GPS network in coastal areas of the United States to generate VLM estimates at all tide-gauge locations (Figure 4.8b). Note that negative values of VLM reflect subsidence while positive values reflect uplift. To determine the VLM contribution to RSL at the coast, the negative and positive direction would be reversed. Broadly, the GPS-based estimates are consistent with the VLM estimates contained in this report. However, when subtracting the VLM rates in this report from the GPS-derived rates, differences become apparent (Figure 4.8c). The largest differences are found along the Southern Alaska coastlines, where rates of uplift are very large, and along the entire Gulf Coast, where subsidence rates are large. The rates are further compared in Figure 4.8d, which again reflects general agreement between the two sets of estimates, although at roughly 75% of the gauges, the tide-gauge-based VLM estimate in this report is greater (less negative in the case of subsidence) than that from GPS. In other words, there are generally higher rates of subsidence indicated in the GPS rates when compared to the VLM estimates in this report.

This comparison with the GPS is not intended to be an assessment of the accuracy of VLM rates and associated projections included in this report. Instead, it highlights some of the challenges associated with both estimating VLM rates at the coast and then projecting these into the future, particularly away from the tide-gauge and GPS stations. The spatial variability and local drivers of VLM are clear in Figure 4.8, and extending the tide-gauge-centered estimates to fill in spatial gaps either through the projection framework in this report or with GPS imaging is challenging to validate, particularly as these methods are not intended to capture VLM varying on small spatial scales. An opportunity is provided, however, by new technologies using satellite-based advanced Interferometric Synthetic Aperture Radar (InSAR) analysis, which can provide higher spatial resolution measurements of VLM rates. Calibrated to land GPS station estimates, measurements of land elevations over time by InSAR are producing VLM rates for large swaths or the U.S. coastal plain (e.g., Bekaert et al., 2017; Buzzanga et al., 2020; Bekaert et al., 2019; all InSAR VLM estimates are publicly available through references). Having a higher-resolution assessment of VLM rates can in turn help communities understand where VLM is now occurring at very fine scales (e.g., street block level) and help make informed decisions of how continued VLM will contribute to future RSL projections. Furthermore, InSAR provides an

⁴³ <https://www.psmsl.org/data/>

additional component to the coastal VLM observing network. Integrated assessments across tide gauges, GPS, and InSAR are likely to be most useful for inferring VLM rates and projecting these rates forward at the spatial scales key to coastal communities. Following is a case study of how the InSAR VLM connects to this VLM-observing network. In general, as there is the possibility of using a user-defined VLM rate within the RSL projections, we examine other sources of VLM that may offer options.

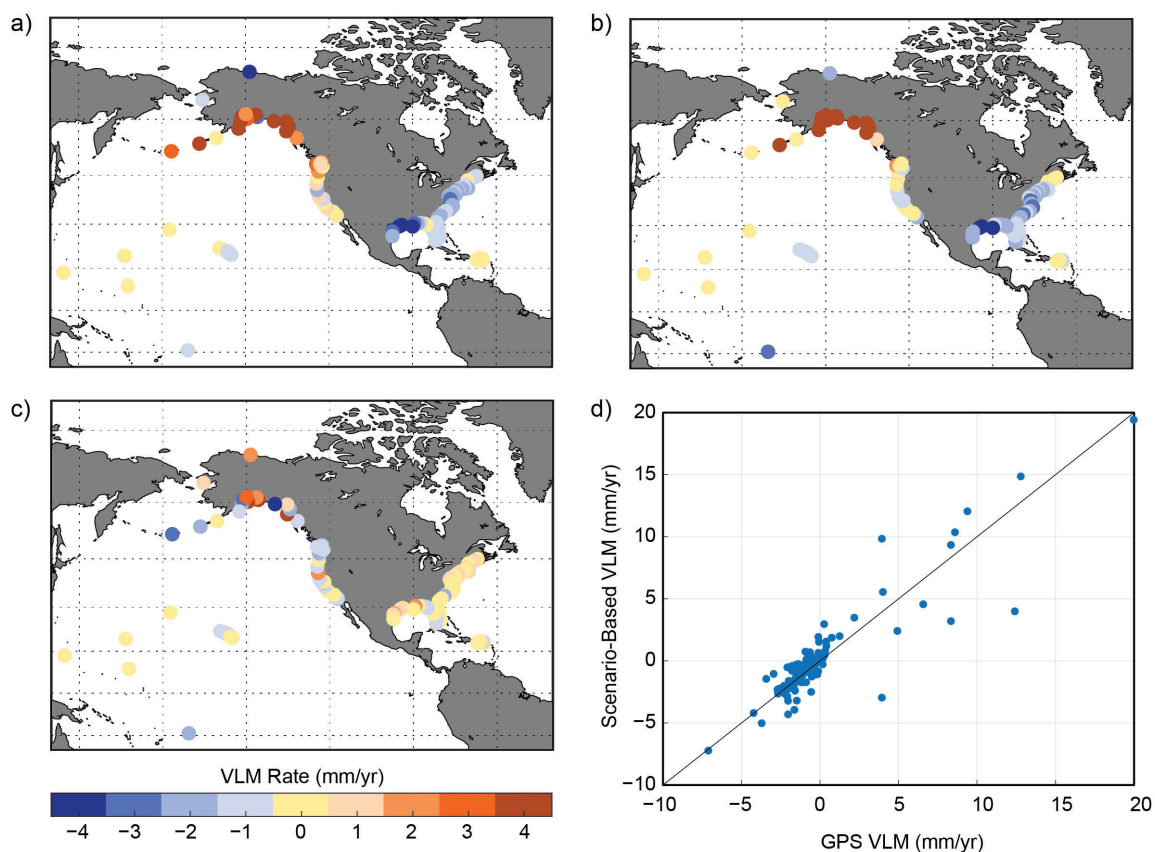


Figure 4.8: Comparison of vertical land motion (VLM) rate estimates (mm/year) from a) the scenario-based framework used in this report, and b) GPS-imaging estimates from Hammond et al. (2021). c) The difference between GPS-derived rates and scenario-derived rates and d) a comparison of the VLM estimates at the U.S. tide-gauge locations are also shown. Negative values of VLM reflect subsidence, while positive values reflect uplift.

Hampton Roads, Virginia

The historical long-term linear RSL rise rate at the Sewells Point, Virginia, tide gauge⁴⁴ is about 4.7 mm/year. More than half of this rate is estimated to be from downward VLM or subsidence with a rate of about 2.9 mm/year, which is close to previous estimates (Zervas, 2013; Kopp et al., 2014; Sweet et al., 2017). This subsidence is driven by both GIA and more localized groundwater withdrawal. If assumed to be linear and persistent into the future, VLM will contribute about 0.29 m to projections of RSL over the next 100 years. For example, by 2050 under the Intermediate-Low and Intermediate scenarios, the amount of RSL rise is projected to be between about 0.4 m and 0.45 m, respectively, with about 35% and 30% of that rise amount, respectively, from VLM.

However, VLM rates across the Hampton Roads region are not uniform. A past study (Eggleston and Pope, 2013) leveraged a variety of in situ observations to find a spatially varying pattern of subsidence ranging from 1.8 to 4.4 mm/year in the region from 1940 to 1971. The variations were connected to groundwater withdrawal in the region, which was captured via this assessment even with an effective spatial resolution on the order of tens of kilometers. More recently, InSAR rate maps have shown a range of subsidence from

⁴⁴ <https://tidesandcurrents.noaa.gov/stationhome.html?id=8638610>

about 1 mm to 5 mm/year in the region over the time period from 2014 to present, with locally higher rates (Figure 4.9; Buzzanga et al., 2020). Importantly, the satellite-based assessment revealed spatial variations on sub-kilometer scales, with some of the most prominent features in the spatial map connected to specific construction projects and land-use changes. With an average rate of subsidence around 3 mm/year over the course of the 21st century, VLM could contribute about 0.3 m to projected RSL, with locally higher amounts elsewhere in the region. Furthermore, comparing the InSAR-derived spatial pattern of VLM to that in either Eggleston and Pope (2013) or the gridded rates in this report provides important information about the linearity of VLM and the timescales on which VLM varies. There are considerable differences between the different assessments, indicating a shift in rates over the time periods considered. While it is necessary to consider the uncertainty in the VLM rate estimates and differences in measurement type, users of VLM information should assess land-use changes over the time periods considered along with the relevant processes driving VLM in the region. InSAR-derived VLM maps will play an increasingly key role in this assessment due to the spatial coverage and resolution provided by the satellites.

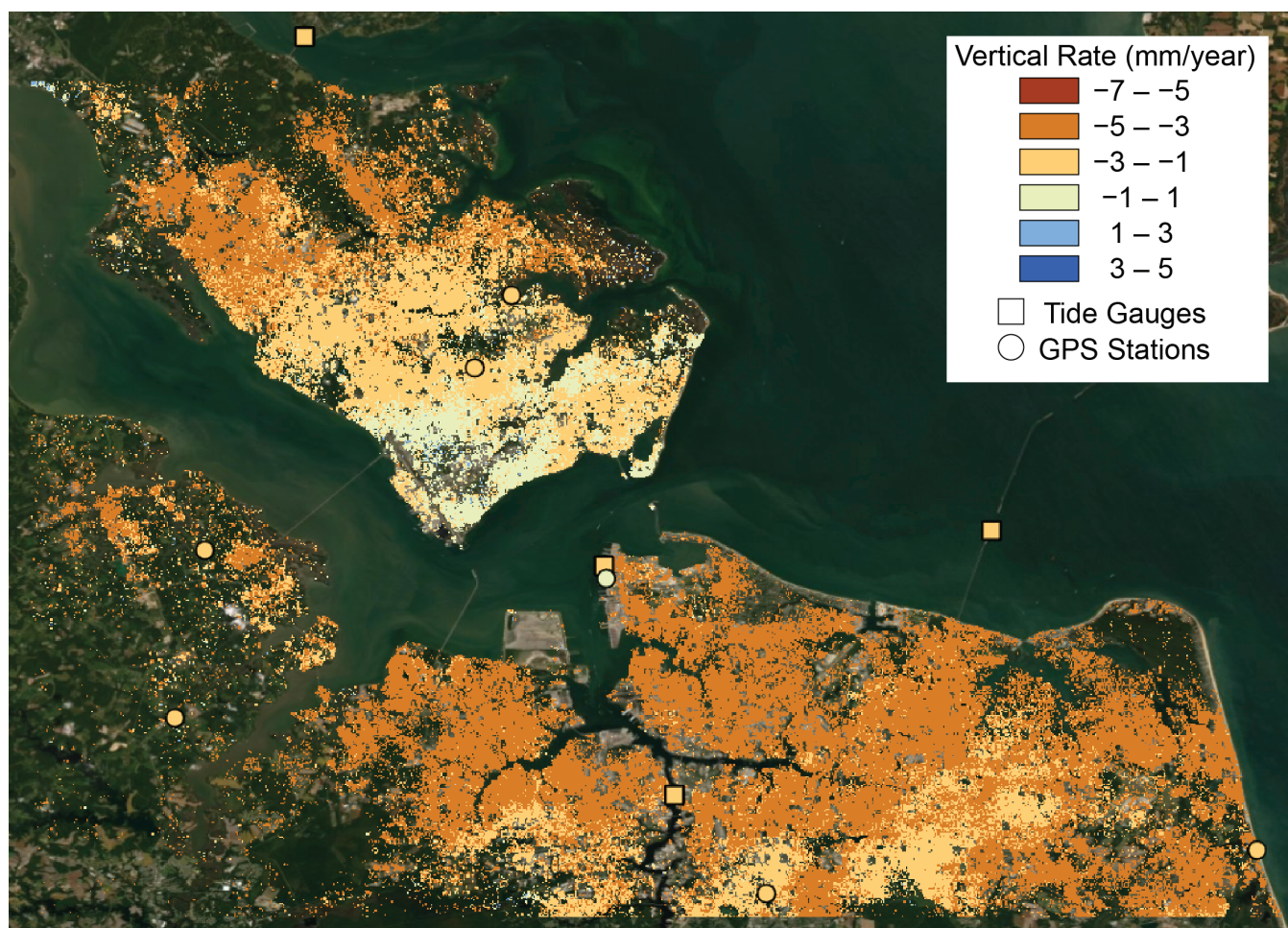


Figure 4.9: Map showing VLM rates (mm/year) for the Hampton Roads region displayed on top of satellite imagery. Higher rates of subsidence are indicated by darker orange colors. Of particular interest is the range of rates in such a small region (e.g., on the order of up to 5 mm/year difference in places). Based on Buzzanga et al. (2020).

Observing and Projecting Coastal Vertical Land Motion

While InSAR-measured VLM provides advantages over other measurement platforms in terms of spatial coverage and resolution, it should be considered in the context of the larger observing network when assessing VLM at the coast. In particular, InSAR serves two potential roles. First, InSAR can be used to provide ongoing monitoring of VLM at high spatial resolutions. InSAR has the potential to generate time series of VLM on a fine spatial scale. Subsidence “hotspots” can be identified along with abrupt shifts in VLM, which can assist in planning and executing adaptation efforts. For coastal communities attempting to alleviate subsidence in their region through efforts such as groundwater reinjection, InSAR provides a potentially better alternative to in situ monitoring to assess the effectiveness of these efforts. Second, InSAR can serve to assess spatial variability in VLM, filling in the gaps between tide gauges and GPS stations in coastal regions. The observations can then be combined in a statistical framework to provide more accurate projections of VLM with better estimates of uncertainty.

Assessing VLM with InSAR is not without challenges, however, although many of these are being addressed in ongoing and planned efforts. First, to be useful for assessing long-term VLM rates with the still relatively short satellite records, the shorter-term VLM rates can be calibrated and tied into the existing National Spatial Reference System (NSRS)⁴⁵ to improve accuracy and representativeness of long-term changes. Second, the availability and coverage of GPS in coastal regions impact the accuracy of VLM by InSAR. To provide a measurement of absolute VLM, InSAR needs to be tied to available GPS measurements. In areas with large gaps between GPS stations, this can lead to reduced accuracy of the InSAR estimates. Ideally, analysis would be conducted to determine optimal GPS station spacing for maintaining integrity of the InSAR-derived velocity field in various environments, including, but not limited to, regions of coastal subsidence, landslide/earthquake/volcanic activity, high plains aquifer depletion, and aquifer depletion in a tectonic area. Finally, InSAR VLM estimates are computationally expensive to perform over large regions, making national coverage a challenge. Efforts are underway, however, to generate a consistent surface displacement product (a preliminary step to estimating VLM) for the United States. A generalized approach for generating absolute VLM estimates from this product could then be created, paving the way for ongoing monitoring of VLM along the U.S. coastlines at high spatial resolutions.

To improve projections of VLM, InSAR alone is not sufficient. Instead, InSAR should be analyzed in tandem with available tide-gauge, GPS, and any other available in situ observations to assess both the spatial variability of VLM rates and potential non-linearities in the VLM rates estimated over these records. These non-linearities are critical for determining the future contribution of VLM to RSL. For example, the long-term rate assessed at a tide gauge as done in this report could differ significantly from the rate of VLM over the past decade because of a sustained land-use change. The comparison between the two types of VLM estimates in Figure 4.9 indicate that these shifts may be present at some locations along the U.S. coastlines and need to be assessed to improve projections of VLM.

⁴⁵ https://oceanservice.noaa.gov/education/tutorial_geodesy/geo08_spatref.html